Chemical Science

ROYAL SOCIETY OF CHEMISTRY

EDGE ARTICLE

View Article Online
View Journal | View Issue

Cite this: *Chem. Sci.*, 2020, **11**, 2394

All publication charges for this article have been paid for by the Royal Society of Chemistry

Received 21st October 2019
Accepted 19th January 2020

DOI: 10.1039/c9sc05299b

rsc.li/chemical-science

Enantioseparation and chiral induction in Ag_{29} nanoclusters with intrinsic chirality†

Hiroto Yoshida,[a] Masahiro Ehara,[*b] U. Deva Priyakumar,[c] Tsuyoshi Kawai[a] and Takuya Nakashima[*a]

The optical activity of a metal nanocluster (NC) is induced either by an asymmetric arrangement of constituents or by a dissymmetric field of a chiral ligand layer. Herein, we unveil the origin of chirality in Ag_{29} NCs, which is attributed to the intrinsically chiral atomic arrangement. The X-ray crystal structure of a $Ag_{29}(BDT)_{12}(TPP)_4$ NC (BDT: 1,3-benzenedithiol; TPP: triphenylphosphine) manifested the presence of intrinsic chirality in the outer shell capping the icosahedral achiral Ag_{13} core. The enantiomers of the $Ag_{29}(BDT)_{12}(TPP)_4$ NC are separated by high-performance liquid chromatography (HPLC) using a chiral column for the first time, showing mirror-image circular dichroism (CD) spectra. The CD spectra are reproduced by time-dependent density functional theory (TDDFT) calculations based on enantiomeric Ag_{29} models with achiral 1,3-propanedithiolate ligands. The mechanism of chiral induction in the synthesis of $Ag_{29}(DHLA)_{12}$ (DHLA: α-dihydrolipoic acid) NCs with a chiral ligand system is further discussed with the aid of DFT calculations. The use of the enantiomeric DHLA ligand preferentially leads to a one-handed atomic arrangement which is more stable than the opposite one, inducing the enantiomeric excess in the population of intrinsically chiral Ag_{29} NCs with CD activity.

Introduction

Chiral metal nanoclusters (NCs) with atomically precise structures have garnered great interest over the recent two decades because of their fascinating structural, electronic and optical properties.[1] Chirality can be introduced into the electronic properties of NCs either by intrinsically chiral atomic arrangements[2–18] or by employing chiral organic ligands such as chiral thiols.[19–25] While intrinsically chiral NCs possess a chiral atomic arrangement in the NC-core including the surface metal-thiolate networks as a stable structure, the use of achiral ligands leads to the formation of a racemic mixture.[2–17] A few studies successfully separated one enantiomer or both enantiomers from the racemic mixture through chiral HPLC columns,[6–8,16] phase transfer with a chiral surfactant,[10] and interaction with chiral reagents and ions.[3b,13] However, there has been no report on the enantioseparation of atomically precise chiral silver NCs, possibly because of reactive and less stable properties of silver NCs compared to gold NCs.[1,26]

Ag_{29} NCs serve as one of the representative examples of atomically precise silver NCs with remarkable photoluminescence properties.[27–30] The X-ray single crystal structure of Ag_{29} NCs was first revealed for $Ag_{29}(BDT)_{12}(TPP)_4$ NCs.[27a] A similar structure and composition were proposed for water soluble silver NCs prepared with bidentate DHLA ligands[29] by mass spectrometry data corresponding to an m/z value corresponding to the $[Ag_{29}(DHLA)_{12}]^{3-}$ composition, exhibiting absorption and photoluminescence spectra similar to those of $Ag_{29}(BDT)_{12}(TPP)_4$ NCs.[29] We have recently imparted optical activity to the NCs by using enantiomeric DHLAs and demonstrated mirror image CD and circular polarized luminescence (CPL) spectra.[30] While the origin of optical activity remained unclear, the chirality analysis of the single crystal structure of the $Ag_{29}(BDT)_{12}(TPP)_4$ NC[27a] by Whetten and co-workers[29d] suggested intrinsic chirality in the shell structure surrounding the icosahedral Ag_{13} core. Their finding motivated us to separate enantiomers of $Ag_{29}(BDT)_{12}(TPP)_4$ NCs which are prepared with achiral ligands and demonstrate chiroptical properties. In this work, the enantiomers of $Ag_{29}(BDT)_{12}(TPP)_4$ NCs are successfully separated with a chiral HPLC column, exhibiting absorption and luminescence spectra identical to those of the racemic mixture but affording mirror image CD spectra. The CD spectra were reproduced by TDDFT calculations based on model NCs employing the 1,3-propanedithiolate ligand in place of BDT. We further discuss the chirality induction mechanism in the synthesis of water soluble analogous $Ag_{29}(DHLA)_{12}$ NCs with the aid of DFT calculations.

[a]*Division of Materials Science, Graduate School of Science and Technology, Nara Institute of Science and Technology (NAIST), Ikoma, Nara 630-01921, Japan. E-mail: ntaku@ms.naist.jp*

[b]*Institute for Molecular Science, Research Center for Computational Science, Myodaiji, Okazaki 444-8585, Japan. E-mail: ehara@ims.ac.jp*

[c]*Centre for Computational Natural Sciences and Bioinformatics, International Institute of Information Technology, Hyderabad 500032, India*

† Electronic supplementary information (ESI) available. See DOI: 10.1039/c9sc05299b

Experimental

Synthesis of $Ag_{29}(BDT)_{12}(TPP)_4$ NCs

$Ag_{29}(BDT)_{12}(TPP)_4$ NCs were prepared according to a method reported in the literature.[27a] For the enantioseparation, the purified NCs were dispersed in ethanol.

Synthesis of Ag_{29}(*R*-DHLA)$_{12}$ NCs

Ag_{29}(*R*-DHLA)$_{12}$ NCs were also prepared according to the reported procedure.[30] The reaction temperature was controlled with a temperature-controlled bath until the formation of Ag_{29} NCs was confirmed with spectroscopic measurements.

Enantioseparation of $Ag_{29}(BDT)_{12}(TPP)_4$ NCs

Enantioseparation of $Ag_{29}(BDT)_{12}(TPP)_4$ NCs was carried out using a JASCO EXTREMA HPLC system equipped with a PU-4180 pump, a UV-4075 detector and a CD-4095 detector. For the enantioseparation, a DAICEL CHILALPAK IA column (5 μm, 4.6 × 250 mm) was used in a JASCO CO-4060 column oven at 20 °C. As a typical condition, 50 μl of ethanol solution (0.02 mg ml^{-1}) was injected and then the separation was performed using ethanol as the eluent at a flow rate of 0.5 ml min^{-1}. The eluting solutions were monitored by optical absorption and a CD signal at 450 nm simultaneously.

Characterization

Electrospray ionization mass (ESI-MS) spectrometry was conducted with a JEOL JMS-T100LC AccuTOF. UV-vis absorption and photoluminescence spectra were recorded with a JASCO V-760 spectrometer and a JASCO FP-8500 spectrofluorometer, respectively. CD spectra were measured on a JASCO J-725 spectropolarimeter.

DFT calculations

DFT and TDDFT calculations were performed for the model Ag_{29} NCs using the B3LYP functional.[31] Relativistic effective core potential LANL2DZ[32] was used for silver atoms and the basis sets of other atoms were 3-21G.[33] For simulating ECD spectra, 200 excited states were solved to cover the spectrum in the energy range up to about 300 nm and the rotatory strength was calculated in the velocity form. All calculations were conducted using the Gaussian 09 suite of programs version E.01.[34]

Results and discussion

$Ag_{29}(BDT)_{12}(TPP)_4$ NCs were prepared according to the method reported by Bakr and co-workers.[27a] The purified NCs were subjected to the HPLC separation study. The HPLC technique was applied to the size-dependent separation of monolayer protected gold NCs,[35] and this technique has been further advanced to achieve high-resolution separation of metal NCs depending on the size, core- and ligand-compositions and coordination isomers.[36,37] While reverse phase HPLC has been mostly used for the polarity-based partitioning of NCs with hydrophobic surface ligands,[37] the separation of enantiomeric NCs with the same composition requires chirality-dependent interactions. Bürgi *et al.* employed a chiral column filled with silica gel tethering aryl-functionalized cellulose as a stationary phase for the enantioseparation of intrinsically chiral gold NCs with the 2-phenylethanethiolate ligand.[6,7] We chose the DAICEL CHILALPAL IA column having aryl-substituted amylose (amylose tris(3,5-dimethylphenyl-carbamate)) in the stationary phase for the separation. The chiral π–π interactions between 3,5-dimethyl units in the stationary phase and phenyl groups on the surface of $Ag_{29}(BDT)_{12}(TPP)_4$ should work as a primary force for the enantioseparation.

The purified NCs were found to be soluble in DMF, ethanol and acetone with moderate polarity but less soluble in acetonitrile, methanol and 1-propanol. When we first tested DMF as a solvent for injection and as a mobile phase, both the enantiomers gave an identical retention time. Since the separation stems from the difference in partition equilibrium between the mobile and stationary phases, the NCs may be too soluble in DMF. We then employed ethanol showing moderate dissolving capability for the NCs. Although the complete separation was not accomplished, two separate peaks at 16.9 and 20 min were confirmed with the UV-vis detector (Fig. 1). The presence of negative and positive signals corresponding to the former and latter peaks in the CD-detected chromatogram clearly demonstrated the successful separation of enantiomers. The separation conditions particularly related to the eluting solvent were further investigated by mixing an additional solvent with ethanol such as DMF, methanol, acetonitrile and hexane. However, all the mixed solvent systems could not much improve the peak separation, resulting in peak broadening or clogging of the column (Fig. S1, ESI†). Therefore, fractions were collected over several separation runs using ethanol and optical properties were measured for the collected fractions.

Each collected ethanol solution was subjected to ESI-MS measurements, providing an *m*/*z* value corresponding to the $[Ag_{29}(BDT)_{12}]^{3-}$ composition with loss of TPP molecules (Fig. S2, ESI†).[27a] The strong π–π interactions between TPP ligands and the aryl groups in the stationary phase may remove them from the surface of NCs since phosphines were reported to weakly bind to the NCs compared to dithiolates.[27a] Meanwhile, UV-vis and photoluminescence spectra of the isolated fraction were identical to those of the racemic mixture before

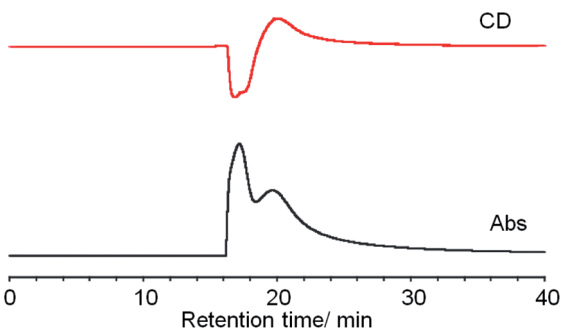

Fig. 1 Simultaneous CD (top) and absorbance (bottom) detected (at 450 nm) chiral HPLC chromatograms of $Ag_{29}(BDT)_{12}(TPP)_4$ NCs.

the HPLC separation, also confirming the preservation of the $Ag_{29}(BDT)_{12}$ NC composition after the separation (Fig. S3, ESI†).

The separated fractions afforded mirror image CD spectra, clearly demonstrating the intrinsic chirality of $Ag_{29}(BDT)_{12}$ NCs having organic ligands with no chiral group (Fig. 2). Very weak first Cotton effect signals were observed around 550 nm with negative and positive signs for the first and second fractions, respectively. Then, each fraction afforded a more prominent CD signal at 460 nm with the same sign as the first Cotton effect. Although the presence of TPP was reported to have little effect on the UV-vis absorption and photoluminescence spectral profiles,[27a] CD spectra were slightly modified by the addition of TPP. Re-dispersion of the separated NCs in DMF resulted in the CD profiles unaltered from those in as-separated ethanol solutions. The prominent changes include a blue-shift by 5–10 nm and the sign-reversal of first Cotton effect signals above 500 nm after the addition of 10 mM TPP (Fig. S4, ESI†). This result further confirmed the loss of TPP molecules and suggested the non-negligible effect of TPP on the electronic structure of NCs contributing to the CD activity. Because the first fraction was less contaminated by the opposite enantiomer,[38] a larger CD amplitude was obtained compared to the second one. We attempted further analysis of each fraction with the chiral HPLC to estimate the enantiomeric excess (ee),[7] whereas it failed because of the low stability of as-separated samples without TPP.[27a] The anisotropy factors ($|g_{abs}| = |\Delta\varepsilon/\varepsilon|$) were therefore estimated tentatively to be no less than 1.1×10^{-3} at 460 nm which is in a similar range to those obtained for Ag_{29}(*R*- or *S*-DHLA)$_{12}$ NCs[30] (1.5×10^{-3} at 500 nm, Fig. S5, ESI†).

To predict the NC structure responsible for each HPLC fraction, TDDFT calculations were performed based on model NCs with 1,3-propanedithiolate ligands. A careful analysis of the single crystal data of $Ag_{29}(BDT)_{12}(TPP)_4$ NCs[27a] suggested that the cubic lattice is composed of both enantiomeric NCs (Fig. S6, ESI†). Both enantiomeric NCs were derived from the crystallographic lattice structure[27a] to construct the model NC enantiomers. The BDT ligands were replaced by 1,3-propanedithiolate and TPP molecules were removed to reduce the computational cost. The loss of TPP ligands was also suggested by the HPLC separation study. The model structures of Ag_{29}(1,3-propanedithiolate)$_{12}^{(3-)}$ were first optimized by the DFT method. Absorption and CD spectra were then simulated based on the ground-state optimized structure. Each optimized enantiomer is composed of a highly symmetric Ag_{13} icosahedral core (Fig. 3a, light blue) and an exterior shell with a chiral atomic arrangement. In the exterior shell, 12 silver atoms capping all 12 silver atoms of the icosahedral Ag_{13} core form four triangles (blue) and the remaining 4 silver atoms (green) face-cap the icosahedral core. These two respective types of silver atoms, *i.e.* triangles and face-capping atoms, in the shell were found to be arranged in a chirally distorted tetrahedral manner as reported by Whetten and co-workers.[29d] Along with the exterior silver atoms, the bidentate ligands are also oriented in a chiral manner. A view with a focus on one of the face-capping silver atoms clearly demonstrates that the bidentate ligands (purple) are arranged in a C_3-symmetry with a right- or left-handed orientation in the Ag(1,3-dithiolate)$_3$ unit (Fig. 3a). It is apparent that, therefore, the chirality of Ag_{29} NCs stems from the asymmetric atomic arrangement in the exterior shell. Meanwhile, the TPP ligands orthogonally cap the center of the Ag(1,3-dithiolate)$_3$ unit in the $Ag_{29}(BDT)_{12}(TPP)_4$ NC in a monodentate manner, having a limited effect on the intrinsically chiral geometry in the exterior shell.

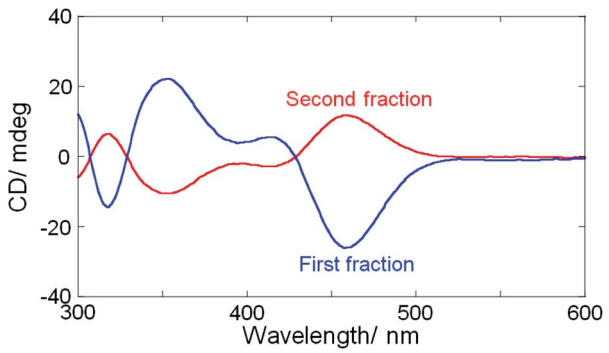

Fig. 2 CD spectra of silver NCs in ethanol after the separation with the chiral column.

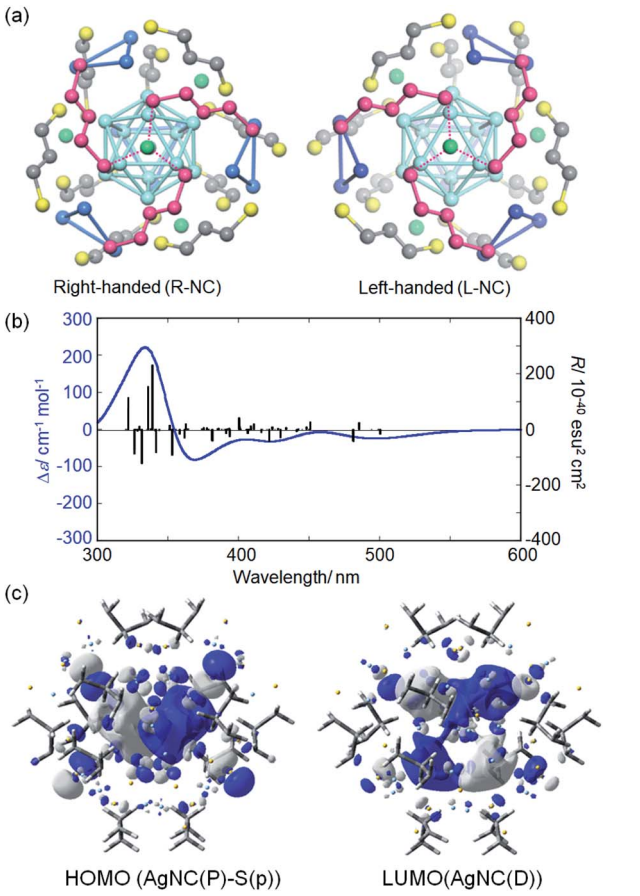

Fig. 3 (a) Optimized structures of enantiomeric Ag_{29}(1,3-propanedithiolate)$_{12}$ model NCs. Hydrogen atoms were omitted for clarity. (b) Simulated CD spectrum based on the R-NC model. (c) Representative HOMO and LUMO orbitals of Ag_{29}(1,3-propanedithiolate)$_{12}^{(3-)}$ (isovalue = 0.02).

The TDDFT calculation based on the ground-state optimized structures simulated the chiroptical properties. Unlike most of the ordinary small molecules, the electronic transitions in NC systems involve a large number of excited states. The model NC with a right-handed ligand orientation (R-NC, Fig. 3a) afforded a CD spectrum similar to that of the first fraction with a small negative first Cotton effect (Fig. 3b and S7† for the simulated UV-vis absorption data), while the one with left-handed orientation (L-NC) resembled that of the second fraction (Fig. S8, ESI†). The deviations of transition energy and rotatory strength (R) between the experimental and simulation data may be attributed to the used functional and basis set in DFT calculations (Fig. S9, ESI†). The triply degenerate lowest state (T symmetry) has a considerable rotatory strength and is characterized by the HOMO–LUMO transitions (Fig. S10 and Table S1, ESI†). The HOMOs (no. 611–613, Fig. S10, ESI†) correspond to the P orbitals of the superatom of the Ag_{13} core and to the p orbitals of helically arranged S atoms, while the LUMOs (LUMO and LUMO+1, no. 614–618) correspond to the D orbitals of the Ag_{13} core. The electronic transitions simulated above 430 nm correspond to the transitions to the LUMOs from the HOMO, HOMO−1 (no. 608–610) and HOMO−3 (no. 603–605), with the considerable contributions of orbitals localized in the chiral shell, suggesting the involvement of charge transfer between the exterior shell and the Ag_{13} core (Fig. S10 and Table S1, ESI†).

The intrinsic chirality of the Ag_{29} NC system was unveiled by the chiral HPLC separation of $Ag_{29}(BDT)_{12}(TPP)_4$ NCs and the DFT calculations based on the Ag_{29}(1,3-propanedithiolate)$_{12}$ NC models. We further discuss the chirality induction mechanism in the synthesis of $Ag_{29}(DHLA)_{12}$ NCs[30] with the aid of DFT calculations. The detailed investigation by de Groot and co-workers[29e] into the synthesis of silver NCs in the presence of racemic DHLA suggested that the composition of $Ag_{29}(DHLA)_{12}$ is formed in an exclusive manner as the most stable structure. Furthermore, the $Ag_{29}(DHLA)_{12}$ NC is expected to have an intrinsic chirality in the structure considering the analogous composition and optical properties to those of $Ag_{29}(BDT)_{12}(TPP)_4$ NCs, whereas its crystal structure has not been obtained yet. It is reasonably assumed that the use of enantiomeric DHLA gives an energy difference between the L- and R-NCs with left- and right-handed ligand orientations, respectively. To gain an insight into this assumption, the DFT calculations were performed.

For the DFT simulation, NC models with right- and left-handed ligand orientations were constructed with employing a mixed ligand system including four (R)-DHLA and eight (R)-butane-1,3-dithiol ligands to reduce the calculation cost (total charge; −7). These ligands were distributed homogeneously so that each Ag(1,3-dithiolate)$_3$ unit focusing on one of the face-capping silver atoms possesses one (R)-DHLA and two (R)-butane-1,3-dithiolate ligands. There are two typical possible orientation patterns in the coordination of 3-position-substituted 1,3-propanedithiolate derivatives for each one-handed NC as shown in Fig. 4. Given the Ag(1,3-dithiolate)$_3$ unit, the dithiolate ligands can coordinate to the central silver atom with a thiolate group either at the 1- or 3-position (Fig. 4). Based on the combinations of the handedness of the NC (L- or R-NC) and ligand coordination orientation, the four possible model NCs were labelled L-1, R-1, L-3 and R-3 NCs (Fig. 4). Among these four patterns, L-1 and R-3 NC models are less stable than others, in which bulky substituents at the 3-position are located outward from the silver center, resulting in higher steric repulsion with an adjacent ligand in the neighboring Ag(1,3-dithiolate)$_3$ unit (see Fig. S11 and Table S2 in the ESI† for the result of Ag_{29}(R-butane-1,3-dithiolate)$_{12}$ models). Therefore, R-1 and L-3 NC models were compared (see Fig. S12 in the ESI† for the entire optimized NC structures). Interestingly, the carboxylate group (COO^-) in the (R)-DHLA ligand was found to coordinate to the central silver atom in each Ag(1,3-dithiolate)$_3$ unit for both models, contributing to the stabilization of the whole NC structure in a similar manner to the role of the TPP ligand in $Ag_{29}(BDT)_{12}(TPP)_4$ NCs.[27] Compared with the R-1 NC, the L-3 NC model was estimated to be more stable by 0.48 kcal mol^{-1}. Thus the left-handed NC was suggested to preferentially form in the presence of (R)-DHLA.

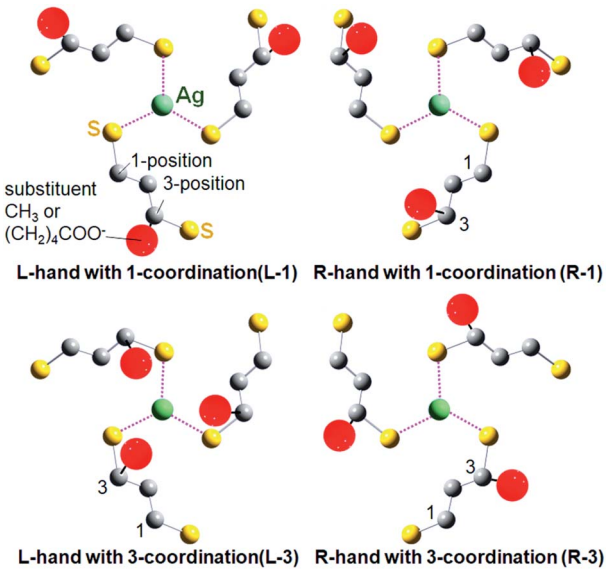

Fig. 4 Four possible combinations between the handedness of the NC and (R)-ligand coordination orientation represented by the face-capping Ag-centered coordination unit (Ag(dithiolate)$_3$ unit) as a part of the NC structure.

To support the calculation reliability, the TDDFT method was applied to the L-3 NC model, simulating absorption and CD spectra. Fig. 5 compares the simulated CD with the experimental data of Ag_{29}(R-DHLA)$_{12}$ NCs.[30] The TDDFT simulation well reproduced the positive first Cotton effect at around 500 nm. The difference between the simulated and experimental spectra can be partly attributed to the simplified ligand structure in the model and the used functional in the DFT calculation. However, it should be noted that the R-1 NC model with the opposite handedness gave the negative first Cotton effect in the same region and a very different CD spectrum from the experimental one (Fig. S13, ESI†). The preferential formation of L-NCs in the presence of (R)-DHLA was thus supported by the CD simulation study with the TDDFT method. A calculation

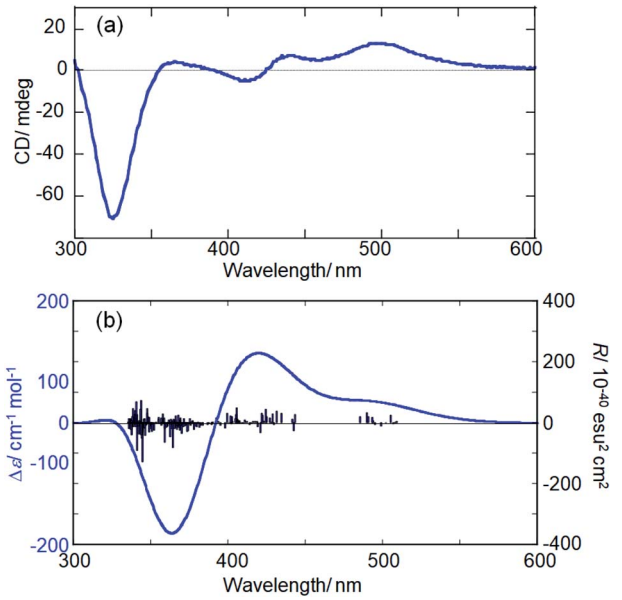

Fig. 5 Experimental (a) and simulated (b) CD spectra of Ag_{29}(*R*-DHLA)$_{12}$ NCs and the L-3 NC model, respectively.

based on the full structure model of Ag_{29}(*R*-DHLA)$_{12}$ might increase the energy difference between the left- and right-handed NCs, whereas it had difficulty with converging by our calculation method.

To gain further insight into the chirality induction mechanism in the Ag_{29}(DHLA)$_{12}$ NCs, the effect of preparation temperature on the enantiomeric excess (ee) of NCs (between the left- and right-handed NCs) was investigated using the enantiopure (*R*)-DHLA ligand. Interestingly, the CD amplitude of Ag_{29}(*R*-DHLA)$_{12}$ NCs increased with increasing preparation temperature (Fig. S14, ESI†). Given that the maximum g_{abs} value of 1.93×10^{-3} (at 500 nm) for Ag_{29}(*R*-DHLA)$_{12}$ NCs prepared at 60 °C corresponds to an ee of 1 (100% selectivity of L-NCs), an enantioselectivity of 80% was estimated for NCs synthesized at 20 °C (90% L-NCs and 10% R-NCs). The ee value further drops to 0.64 at 10 °C (82% L-NCs and 18% R-NCs). A small energy difference between the most stable L-NCs and the second most stable R-NCs resulted in the formation of NCs with both handedness even with the use of a homochiral (*R*)-ligand, which is in accordance with the DFT calculation result. The formation of Ag_{29} NCs is considered to involve the nucleation of larger size nanoparticles and the subsequent size-focusing processes.[29e] The rapid nucleation process should proceed *via* a kinetically controlled reduction reaction while the size-focusing one occurs with oxidation-assisted etching of larger size nanoparticles.[29e] Temperature should have a more prominent effect on the latter process than the former one, introducing thermodynamic controllability in the formation of NCs. Therefore, the increase of ee with increasing preparation temperature suggested the presence of a considerable activation barrier in the chirality inversion[39] between the L- and R-NCs. That is, the increase in the preparation temperature facilitates the introduction of thermodynamic control in the formation of NCs, resulting in the distribution between the R- and L-NCs on the basis of energy difference ($\Delta\Delta H$, Fig. S15, ESI†). We further investigated the possibility of chirality inversion after the completion of NC formation. The Ag_{29}(*R*-DHLA)$_{12}$ NCs prepared at 10 °C with relatively low purity of NC-handedness (g_{abs} at 500 nm = 1.2×10^{-3}) were treated at 60 °C for 90 min, resulting in the increase of the g_{abs} value up to 1.7×10^{-3} (Fig. S14, ESI†). This result indicated the inversion of R-NCs to L-NCs with a more thermodynamically stable structure upon heating. The chirality inversion requires the rearrangement of bidentate ligand orientation in the exterior shell, which should serve as one of the origins of the activation barrier.[39] Meanwhile, further increase in the preparation temperature (>70 °C) impaired the stability of NCs, decreasing the net g_{abs} value.

Conclusions

In summary, we have succeeded in the enantioseparation of intrinsically chiral $Ag_{29}(BDT)_{12}(TPP)_4$ NCs with a chiral HPLC method and the separated fractions afforded mirror image CD spectra. The DFT-optimized models clearly demonstrated the emergence of the chiral structure in the atomic arrangement in the exterior shell surrounding the icosahedral Ag_{13} core. The TDDFT calculation based on the model structure revealed that the optical activity stems from the electronic transition between the molecular orbitals delocalized in the whole NCs including the ligand-shell layer. The use of an enantiomeric ligand such as DHLA successfully led to the preferential formation of one-handed intrinsically chiral NCs, which was supported by the DFT calculations giving an energy difference between the right- and left-handed NCs with employing a homochiral ligand system. The chiral NCs with a precise atomic structure are expected to serve as a platform to work on with functional ligand assemblies with a precise chiral orientation on the NC.

Conflicts of interest

There are no conflicts to declare.

Acknowledgements

This work was supported by JSPS KAKENHI grant numbers JP16H06522 (T. N.) and 16H06511 (M. E.) in Scientific Research on Innovative Area, "Coordination Asymmetry". We are grateful to Ms Yoshiko Nishikawa for her support in the ESI-MS measurement.

Notes and references

1 (*a*) C. Noguez and I. L. Garzón, *Chem. Soc. Rev.*, 2009, **38**, 757–771; (*b*) Y. Wang, J. Xu, Y. Wang and H. Chen, *Chem. Soc. Rev.*, 2013, **42**, 2930–2962; (*c*) S. Knoppe and T. Bürgi, *Acc. Chem. Res.*, 2014, **47**, 1318–1326; (*d*) T. Bürgi, *Nanoscale*, 2015, **7**, 15553–15567; (*e*) J. Kumar, K. G. Thomas and L. M. Liz-Marzán, *Chem. Commun.*, 2016, **52**, 12555–12569; (*f*) W. Ma, L. Xu, A. F. de Moura, X. Wu, H. Kuang, C. Xu and N. A. Kotov, *Chem. Rev.*, 2017, **117**, 8041–8093; (*g*)

I. Chakraborty and T. Pradeep, *Chem. Rev.*, 2017, **117**, 8208–8271; (*h*) C. Zeng and R. Jin, *Chem.–Asian J.*, 2017, **12**, 1839–1850; (*i*) N. V. Karimova and C. M. Aikens, *Part. Part. Syst. Charact.*, 2019, **36**, 1900043.

2 C. Zeng, C. Liu, Y. Chen, N. L. Rosi and R. Jin, *J. Am. Chem. Soc.*, 2014, **136**, 11922–11925.

3 (*a*) X.-K. Wan, S.-F. Yuan, Z.-W. Lin and Q.-M. Wang, *Angew. Chem., Int. Ed.*, 2014, **53**, 2923–2926; (*b*) Y. Zhu, H. Wang, K. Wan, J. Guo, C. He, Y. Yu, L. Zhao, Y. Zhang, J. Lv, L. Shi, R. Jin, X. Zhang, X. Shi and Z. Tang, *Angew. Chem., Int. Ed.*, 2018, **57**, 9059–9063.

4 C. Zeng, T. Li, A. Das, N. L. Rosi and R. Jin, *J. Am. Chem. Soc.*, 2013, **135**, 10011–10013.

5 (*a*) O. Lopez-Acevedo, H. Tsunoyama, T. Tsukuda, H. Häkkinen and C. M. Aikens, *J. Am. Chem. Soc.*, 2010, **132**, 8210–8218; (*b*) H. Qian, W. T. Eckenhoff, Y. Zhu, T. Pintauer and R. Jin, *J. Am. Chem. Soc.*, 2010, **132**, 8280–8281.

6 I. Dolamic, S. Knoppe, A. Dass and T. Bürgi, *Nat. Commun.*, 2012, **3**, 798.

7 S. Knoppe, I. Dolamic, A. Dass and T. Bürgi, *Angew. Chem., Int. Ed.*, 2012, **51**, 7589–7591.

8 C. Zeng, T. Li, A. Das, N. L. Rosi and R. Jin, *J. Am. Chem. Soc.*, 2013, **135**, 10011–10013.

9 P. D. Jadzinsky, G. Calero, C. J. Ackerson, D. A. Bushnell and R. D. Kornberg, *Science*, 2007, **318**, 430–433.

10 S. Knoppe, O. A. Wong, S. Malola, H. Hakkinen, T. Bürgi, T. Verbiest and C. J. Ackerson, *J. Am. Chem. Soc.*, 2014, **136**, 4129–4132.

11 (*a*) C. Zeng, Y. Chen, K. Kirschbaum, K. J. Lambright and R. Jin, *Science*, 2016, **354**, 1580–1584; (*b*) C. Zeng, Y. Chen, K. Kirschbaum, K. Appavoo, M. Y. Sfeir and R. Jin, *Sci. Adv.*, 2015, **1**, e1500045.

12 F. Tian and R. Chen, *J. Am. Chem. Soc.*, 2019, **141**, 7107–7114.

13 J. Yan, H. Su, H. Yang, C. Hu, S. Malola, S. Lin, B. K. Teo, H. Häkkinen and N. Zheng, *J. Am. Chem. Soc.*, 2016, **138**, 12751–12754.

14 H. Yang, J. Yan, Y. Wang, G. Deng, H. Su, X. Zhao, C. Xu, B. K. Teo and N. Zheng, *J. Am. Chem. Soc.*, 2017, **139**, 16113–16116.

15 C. Liu, T. Li, H. Abroshan, Z. Li, C. Zhang, H. J. Kim, G. Li and R. Jin, *Nat. Commun.*, 2018, **9**, 744.

16 S. Jin, F. Xu, W. Du, X. Kang, S. Chen, J. Zhang, X. Li, D. Hu, S. Wang and M. Zhu, *Inorg. Chem.*, 2018, **57**, 5114–5119.

17 R. S. Dhayal, Y. R. Lin, J. H. Liao, Y. J. Chen, Y. C. Liu, M. H. Chiang, S. Kahlal, J. Y. Saillard and C. W. Liu, *Chem.–Eur. J.*, 2016, **22**, 9943–9947.

18 B. Li, Y. J. Kong, S. Li, X. F. Liu, P. Luo and S. Q. Zang, *Part. Part. Syst. Charact.*, 2019, **36**, 1900069.

19 (*a*) T. G. Schaaff, G. Knight, M. N. Shafigullin, R. F. Borkman and R. L. Whetten, *J. Phys. Chem. B*, 1998, **102**, 10643–10646; (*b*) T. G. Schaaff and R. L. Whetten, *J. Phys. Chem. B*, 2000, **104**, 2630–2641.

20 H. Yao, K. Miki, N. Nishida, A. Sasaki and K. Kimura, *J. Am. Chem. Soc.*, 2005, **127**, 15536–15543.

21 M. Zhu, H. Qian, X. Meng, S. Jin, Z. Wu and R. Jin, *Nano Lett.*, 2011, **11**, 3963–3969.

22 (*a*) N. Nishida, H. Yao, T. Ueda, A. Sasaki and K. Kimura, *Chem. Mater.*, 2007, **19**, 2831–2841; (*b*) N. Cathcart, P. Mistry, C. Makra, B. Pietrobon, N. Coombs, M. Jelokhani-Niaraki and V. Kitaev, *Langmuir*, 2009, **25**, 5840–5846; (*c*) M. Farrag, M. Tschurl and U. Heiz, *Chem. Mater.*, 2013, **25**, 862–870.

23 H. Yao, M. Saeki and K. Kimura, *J. Phys. Chem. C*, 2010, **114**, 15909–15915.

24 A. Sánchez-Castillo, C. Noguez and I. L. Garzón, *J. Am. Chem. Soc.*, 2010, **132**, 1504–1505.

25 H. Yao, *Prog. Nat. Sci.: Mater. Int.*, 2016, **26**, 428–439.

26 R. Jin, S. Zhao, Y. Xing and R. Jin, *CrystEngComm*, 2016, **18**, 3996–4005.

27 (*a*) L. G. AbdulHalim, M. S. Bootharaju, Q. Tang, S. Del Gobbo, R. G. AbdulHalim, M. Eddaoudi, D. E. Jiang and O. M. Bakr, *J. Am. Chem. Soc.*, 2015, **137**, 11970–11975; (*b*) X. Kang, S. Wang and M. Zhu, *Chem. Sci.*, 2018, **9**, 3062–3068; (*c*) A. Nag, P. Chakraborty, M. Bodiuzzaman, T. Ahuja, S. Antharjanam and T. Pradeep, *Nanoscale*, 2018, **10**, 9851–9855; (*d*) X. Wei, X. Kang, Q. Yuan, C. Qin, S. Jin, S. Wang and M. Zhu, *Chem. Mater.*, 2019, **31**, 4945–4952.

28 (*a*) B. Adhikari and A. Banerjee, *Chem. Mater.*, 2010, **22**, 4364–4371; (*b*) W. T. Chen, Y. J. Hsu and P. V. Kamat, *J. Phys. Chem. Lett.*, 2012, **3**, 2493–2499; (*c*) P. T. Chin, M. van der Linden, E. J. van Harten, A. Barendregt, M. T. Rood, A. J. Koster, F. W. van Leeuwen, C. de Mello Donega, A. J. Heck and A. Meijerink, *Nanotechnology*, 2013, **24**, 075703.

29 (*a*) I. Russier-Antoine, F. Bertorelle, R. Hamouda, D. Rayane, P. Dugourd, Z. Sanader, V. Bonacic-Koutecky, P. F. Brevet and R. Antoine, *Nanoscale*, 2016, **8**, 2892–2898; (*b*) M. van der Linden, A. Barendregt, A. J. van Bunningen, P. T. Chin, D. Thies-Weesie, F. M. de Groot and A. Meijerink, *Nanoscale*, 2016, **8**, 19901–19909; (*c*) D. M. Black, G. Robles, P. Lopez, S. B. H. Bach, M. Alvarez and R. L. Whetten, *Anal. Chem.*, 2018, **90**, 2010–2017; (*d*) P. Lopez, H. H. Lara, S. M. Mullins, D. M. Black, H. M. Ramsower, M. M. Alvarez, T. L. Williams, X. Lopez-Lozano, H.-C. Weissker, A. P. García, I. L. Garzón, B. Demeler, J. L. Lopez-Ribot, M. J. Yacamán and R. L. Whetten, *ACS Appl. Nano Mater.*, 2018, **1**, 1595–1602; (*e*) M. van der Linden, A. J. van Bunningen, M. U. Delgado-Jaime, B. Detlefs, P. Glatzel, A. Longo and F. M. F. de Groot, *J. Phys. Chem. C*, 2018, **122**, 28351–28361.

30 J. Kumar, T. Kawai and T. Nakashima, *Chem. Commun.*, 2017, **53**, 1269–1272.

31 A. D. Becke, *J. Chem. Phys.*, 1993, **98**, 5648–5652.

32 P. J. Hay and W. R. Wadt, *J. Chem. Phys.*, 1985, **82**, 270–283.

33 J. S. Binkley, J. A. Pople and W. J. Hehre, *J. Am. Chem. Soc.*, 1980, **102**, 939–947.

34 M. J. Frisch, G. W. Trucks, H. B. Schlegel, G. E. Scuseria, M. A. Robb, J. R. Cheeseman, G. Scalmani, V. Barone, B. Mennucci and G. A. Petersson, *et al.*, *Gaussian 09*, Wallingford, CT, 2009.

35 V. L. Jimenez, M. C. Leopold, C. Mazzitelli, J. W. Jorgenson and R. W. Murray, *Anal. Chem.*, 2003, **75**, 199–206.

36 (*a*) Y. Negishi, C. Sakamoto, T. Ohyama and T. Tsukuda, *J. Phys. Chem. Lett.*, 2012, **3**, 1624–1628; (*b*) Y. Niihori, M. Matsuzaki, T. Pradeep and Y. Negishi, *J. Am. Chem. Soc.*, 2013, **135**, 4946–4949; (*c*) Y. Niihori, Y. Kikuchi, A. Kato, M. Matsuzaki and Y. Negishi, *ACS Nano*, 2015, **9**, 9347–9356; (*d*) Y. Niihori, Y. Koyama, S. Watanabe, S. Hashimoto, S. Hossain, L. V. Nair, B. Kumar, W. Kurashige and Y. Negishi, *J. Phys. Chem. Lett.*, 2018, **9**, 4930–4934.

37 (*a*) Y. Niihori, C. Uchida, W. Kurashige and Y. Negishi, *Phys. Chem. Chem. Phys.*, 2016, **18**, 4251–4265; (*b*) Y. Niihori, K. Yoshida, S. Hossain, W. Kurashige and Y. Negishi, *Bull. Chem. Soc. Jpn.*, 2019, **92**, 664–695.

38 K. Shimomura, T. Ikai, S. Kanoh, E. Yashima and K. Maeda, *Nat. Chem.*, 2014, **6**, 429–434.

39 (*a*) S. Knoppe, I. Dolamic and T. Bürgi, *J. Am. Chem. Soc.*, 2012, **134**, 13114–13120; (*b*) B. Varnholt, I. Dolamic, S. Knoppe and T. Bürgi, *Nanoscale*, 2013, **5**, 9568–9571.